Fabrication of antibacterial and biomimetic chitosan-based hydrogel embedded with Ag/MXene nanocomposites as photothermal centers for solar steam generation and desalination

Shuyan Hao[1], Xintong Chen[1], Tingting Zhao[1], Yanyan Jiang[1], Hecheng Han[1], Jiurong Liu[1], Lun Dong[2], and Fenglong Wang[1]

[1]Shandong University
[2]Qilu Hospital of Shandong University

March 10, 2023

Abstract

Solar-driven interfacial steam generation is considered as a sustainable and cost-effective approach to produce freshwater from seawater or sewage, whereas unavoidable microbial contamination and low evaporation efficiency remain challenges. Herein, we report a high-performance and antibacterial 3D Ag/MXene@chitosan hydrogel (described as AM/Ch gel) evaporator through incorporation of two-dimensional (2D) Ag/MXene composites into three-dimensional (3D) chitosan hydrogel. Thanks to the synergistic contributions from chitosan hydrogel matrix and Ag/MXene composites, 3D AM/Ch gel could completely eradicate both E. coli and S. aureus under simulated solar light irradiation, ensuring the production of microbial-free drinkable water. Benefiting from the superb photo-to-thermal conversion behavior and feasible water transportation in the 3D networks, the prepared AM/Ch gel-based evaporator exhibits intriguing solar steam generation performances, with evaporation rate and solar energy utilization efficiency of 3.22 kg m–2 h–1 and 94.9% under irradiation of 0.2 W cm–2, respectively. As a demonstration, the quality of collected liquid water evaporated from seawater adopted from the Yellow Sea, China, well satisfies the requirement for drinking water from World Health Organization. Moreover, the AM/Ch gel exhibits high flexibility and chemical stability, excellent dye molecules adsorption capacity and self-cleaning ability, indicating its promising potential for durable and sustainable water distillation.

Fabrication ofantibacterialand biomimetic chitosan-based hydrogel embedded with Ag/MXene nanocomposites as photothermal centers for solar steam generation and desalination

Shuyan Hao[1,#], Xintong Chen[1,#], Tingting Zhao[1], Yanyan Jiang[1], Hecheng Han[1], Jiurong Liu[1], Lun Dong[2,4], Fenglong Wang[1,3,*]*

[1] Key Laboratory for Liquid-Solid Structural Evolution and Processing of Materials Ministry of Education, Shandong University, Jinan 250061, P. R. China

[2] Department of Breast Surgery, Qilu Hospital, Shandong University, Jinan, Shandong Province, China.

[3] Shenzhen Research Institute of Shandong University, Shenzhen, Guangdong, 518057, China.

[4] Department of Pharmacology, School of Medicine, Shandong University, Jinan 250012, China.

***Corresponding Authors' Emails:**

fenglong.wang@sdu.edu.cn (F.L.W)

donglun@email.sdu.edu.cn (L.D)

Keywords: Ag/MXene composites, chitosan hydrogels, solar evaporator, antibacterial effect, photothermal materials

Solar-driven interfacial steam generation is considered as a sustainable and cost-effective approach to produce freshwater from seawater or sewage, whereas unavoidable microbial contamination and low evaporation efficiency remain challenges. Herein, we report a high-performance and antibacterial 3D Ag/MXene@chitosan hydrogel (described as AM/Ch gel) evaporator through incorporation of two-dimensional (2D) Ag/MXene composites into three-dimensional (3D) chitosan hydrogel. Thanks to the synergistic contributions from chitosan hydrogel matrix and Ag/MXene composites, 3D AM/Ch gel could completely eradicate both*E. coli* and *S. aureus*under simulated solar light irradiation, ensuring the production of microbial-free drinkable water. Benefiting from the superb photo-to-thermal conversion behavior and feasible water transportation in the 3D networks, the prepared AM/Ch gel-based evaporator exhibits intriguing solar steam generation performances, with evaporation rate and solar energy utilization efficiency of 3.22 kg m^{-2} h^{-1} and 94.9% under irradiation of 0.2 W cm^{-2}, respectively. As a demonstration, the quality of collected liquid water evaporated from seawater adopted from the Yellow Sea, China, well satisfies the requirement for drinking water from World Health Organization. Moreover, the AM/Ch gel exhibits high flexibility and chemical stability, excellent dye molecules adsorption capacity and self-cleaning ability, indicating its promising potential for durable and sustainable water distillation.

1. Introduction

The rapid growth of the world population results in freshwater scarcity one of the most problematic issues in the twenty-first century.[1,2]Besides, the ever-accelerated development of industry brings about severe environmental pollution, especially in developing countries or some rural regions, further making the lack of clean water a sharp problem.[3-5] In addition, the emergence of drug-resistant bacteria in water resources due to antibiotics abuse has also become a significant obstacle to the clean water supply.[6,7]Conventional clean water production approaches include chemical precipitation, ozone and ultraviolet radiation, membrane filtration, and chlorine-containing disinfectants cleaning, whereas these energy-intensive technologies may lead to high environmental pressure and harmful by-products during the disinfection process.[8,9]Moreover, the water supply infrastructure installation and maintenance in remote areas are unrealistic to some extent ascribed to the high cost and low utilization efficiency.[8] Thus, exploiting innovative clean water production technologies is highly desirable to guarantee the safe water supply.

With the advance of photothermal technologies, the solar-driven interfacial water evaporation process, in which the steam is generated just at the interfaces between the photothermal materials and water, exhibits the feature of enhanced heat utilization and evaporation efficiency, flexible portability, low cost and feasible installation, compared with the conventional passive sea water desalination, and thus has emerged as an up-and-coming technology for seawater desalination and wastewater treatment.[10-12]Except for the heat localization concerns in the solar evaporation process, the solar-driven steam generation efficiency largely depends on the microstructure and components of photothermal materials. Thus, up to now, tremendous attention has been paid to the preparation of plasmonic nanoparticles,[13]conjugated polymers,[14]semiconductors,[15,16]carbon-based materials,[17,18]aerogels,[19,20] and hydrogels[21,22] for potential solar desalination. Among these investigated solar steam generators, photothermal hydrogels in which photothermal materials as "micro-heaters" are accommodated to induce solar-powered water evaporation, enjoying the merits of low cost, feasible fabrication and high efficiency, have shown bright prospects in water transportation and vapor production as they could modulate the intriguing water molecule interaction states by forming hydrogen bonds between water molecules and polymer chains which lowers the vaporization enthalpy.[23] Besides, numerous water-containing pores are advantageous for enhancing the multiple reflections of incident photons, which also enhances the solar energy utilization efficiency.[20]

On the other side, MXenes, a developing family of 2D materials, have drawn increased interest due to their potential in energy storage, water desalination, light-to-heat conversion, electromagnetic shielding and

photocatalysis.[24,25] Moreover, they could be readily integrated into hydrogel skeletons to form various functional hybrid nanostructures.[26,27] Besides, the layered architecture of MXenes is also beneficial for the perturbation of hydrogen bonding among water molecules, and thus, lower evaporation enthalpy could be anticipated.[28,29]Lu et al. created a 2D nanostructure-embedded hybrid hydrogel by simultaneously interpenetrating few-layer MXenes and reduced graphene oxide nanosheets into polymer networks, showing a high evaporation efficiency of up to 83.5% under one sun illumination.[21] In addition, due to its superb photothermal performance, MXenes also exhibit promising antibacterial properties under light irradiation, which conduces to the pathogen-free water supply.[24] Given that the photothermal antibacterial effect of MXenes could only be triggered with the presence of light irradiation and the sterilization efficiency of chitosan to drug-resistant microbial is rather weak, it is envisioned that by rationally embedding the 2D-structured MXene nanosheets loaded with strong antibacterial agents into chitosan hydrogel matrix, optimized vaporization enthalpy and enhanced bacterial eradiation effect could be expected.

Based on the above analysis, in this work, we successfully prepared Ag/MXene nanosheets with optimized mass ratios and incorporated them into chitosan hydrogel, forming Ag/MXene@chitosan hydrogel composites as an efficient interfacial solar steam generator. In the porous architecture, Ag/MXene nanocomposites acted as photothermal centers for the solar steam generation and chitosan hydrogel platform, with abundant water-enriched pores in micrometer scale, ensured the continuous water transportation to the evaporation sites. Therefore, an attractive evaporation rate of 3.22 kg m^{-2} $h^{-1}$with light energy conversion efficiency of 94.9% was achieved, which exceeded the majority of previously reported photothermal evaporators. By examining the concentrations of main ions (Na^+, Mg^{2+}, K^+, and Ca^{2+}) in the distilled water samples from the Yellow Sea, China, it was found that their concentrations were drastically reduced after desalination with the evaporator, meeting the standard of drinking water according to the World Health Organization. The hydrogel also exhibited a high capacity for dye-contaminated water purification, showing its versatile application potential for various water cleaning purposes. Furthermore, the synergistic contributions from the uniformly dispersed Ag nanoparticles (ca. 3˜12nm), MXene nanosheets and chitosan chains endowed the Ag/MXene@chitosan hydrogel with excellent photo-induced antibacterial performances towards*S.aureus* and *E.coli* , revealing its potential for pathogen-free water production. Moreover, the intrinsic bactericidal ability of chitosan and the Ag^+ ions release brought about antibacterial self-cleaning properties to the hydrogel generator, benefiting its durability for long-term use. In summary, our work provides a new strategy for designing cost-effective, highly portable and environmentally friendly hydrogel-based solar evaporators for bacteria-free freshwater supply.

2. Results and Discussion

2.1. Characterizations of Materials

The Ag/MXene@chitosan hydrogel was prepared by bulk MAX etching to produce MXene nanosheets, Ag/MXene composited sheets preparation and their incorporation into chitosan hydrogel, as depicted in **Figure 1** a. In detail, MXene nanosheets (Figure S1a-b, Supporting Information) were obtained by etching out the aluminum layer of MAX bulk phase (Figure S2a-e, Supporting Information) with a LiF/HCl mixture solution as etchants. After Ag nanoparticles deposition, from the scanning electron microscope (SEM) image and corresponding energy-dispersive X-ray spectroscopy (EDS) elemental mappings of $Ag_{0.2}/MXene_{0.8}$, it could be observed that the layered structure of MXene maintained and Ag nanoparticles were evenly distributed on the surface of MXene nanosheets (Figure 1b-d). The transmission electron microscopy (TEM) image of the $Ag_{0.2}/MXene_{0.8}$ further demonstrated that Ag nanoparticles with a size of 3˜12 nm were uniformly decorated on the $Ti_3C_2T_x$layers (Figure 1e). Meanwhile, the high-resolution TEM (HRTEM) images showed that the lattice fringe with an interplanar spacing of 0.236 nm corresponded to the (111) plane of Ag nanoparticles (Figure 1f). Phase structure of the produced Ag/MXene composited nanosheets with various mass ratios were validated by the X-ray diffraction (XRD) patterns (Figure 1g). It was clear that $Ti_3C_2T_x$ had been successfully prepared, as evidenced by the distinctive peak at $2\vartheta = 6.1°$. The characteristic peaks at $2\vartheta = 38.2°$, 44.4°, 64.6°, 77.6°, and 81.8° of the Ag/MXene composites could be assigned to the (111), (200), (220), (311), and (222) planes of Ag (JCPDS no. 87-0720), respectively. To optimize the

loading of Ag nanoparticles (NPs), we prepared a series of Ag/MXene nanocomposites with various mass ratios. It was worth noting that when the relative proportion of Ag NPs was higher than 20 wt.%, the 2D morphology of MXene was destroyed, which might be attributed to the oxidation effect from silver nitrate (Figure S3a, Supporting Information).[30] Thus $Ag_{0.2}/MXene_{0.8}$ composite nanosheets were selected for the fabrication of AM/Ch gel. The survey scan X-ray photoelectron spectroscopy (XPS) spectra of pure MXene and $Ag_{0.2}/MXene_{0.8}$ were shown in Figure 1h, in which characteristic peaks originating from Ti 2p, C 1s, O 1s, F 1s, and Cl 2p orbitals could be observed. The peak at 368.5 eV in the composites could be assigned to the Ag $3d_{5/2}$ orbital, supporting the successful loading of Ag nanoparticles on the Ti_3C_2Tx layers. As shown in the high-resolution Ti 2p spectra (Figure 1i), the peaks of Ti species on the surface of $Ag_{0.2}/MXene_{0.8}$ changed from a low valence state to a higher valence state (Ti^{2+}, Ti^{3+} - Ti^{4+}) after Ag decoration, which further corroborated that the introduced silver nitrate oxidized the highly reducing Ti ions on the surface and this was believed to benefit the stability of MXene sheets.[31] In the core-level Ag 3d doublet spectrum (Figure 1j), the characteristic peaks at 374.51 eV and 368.51 eV could be indexed to Ag $3d_{3/2}$ and Ag $3d_{5/2}$ orbitals, and the splitting between the two distinctive peaks was 6.0 eV, demonstrating the existence of metallic Ag NPs in the $Ag_{0.2}/MXene_{0.8}$.

AM/Ch gel was synthesized by cross-linking chitosan chains through hydrogen bonding with $Ag_{0.2}/MXene_{0.8}$ as additives. As shown in Figure S4a-c (Supporting Information), after cross-linking, the fluidity of the added solution disappeared. Figure 1k showed cross-sectional SEM images of freeze-dried AM/Ch gel, demonstrating the porous networking structure, which was believed to enhance the water transportation during the solar steam generation process. AM/Ch gel also showed adhesive features and high stability (Figure S5a-b, Supporting Information). Additionally, the shape and size of the AM/Ch gel could be readily manipulated by changing the shape of mould, and in our case, we fabricated a toy rabbit with white chitosan hydrogel (described as Ch gel) as body and black AM/Ch gel as eyes, indicating the high flexibility of the hydrogel for various application purposes (Figure 1l). The phase structure of hydrogel samples after being freeze-dried was analysed using XRD (Figure 1m). The peaks at 2ϑ = 6.1°, 38.20°, 44.40°, 64.60°, 77.60°, and 81.76° of frozen AM/Ch gel could be attributed to above-mentioned characteristic peaks of $Ti_3C_2T_x$ and Ag nanoparticles. In addition, the peak intensity of chitosan significantly decreased after cross-linking, which could be attributed to the reduced crystallinity. All these texture property characterizations clearly indicated the successful fabrication of flexible AM/Ch gel.

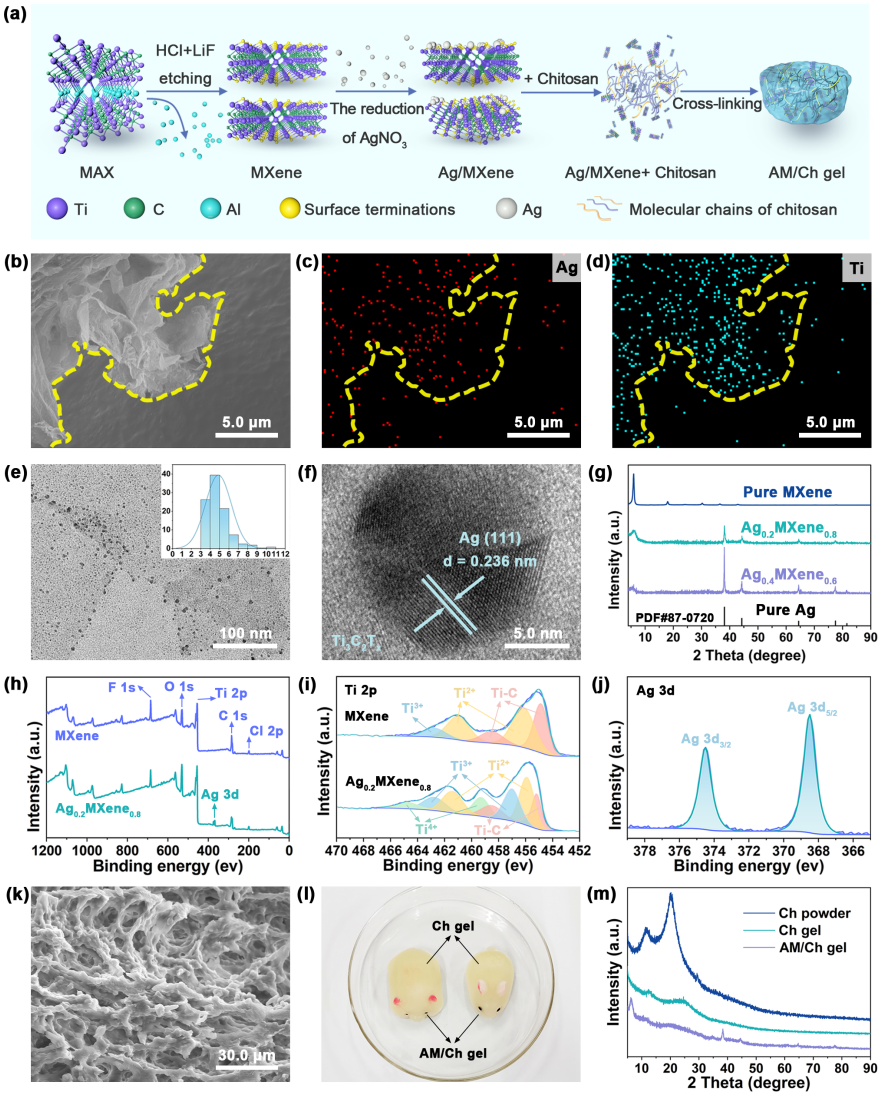

Figure 1. (a) Schematic illustration of the fabrication process of the AM/Ch gel. SEM image of $Ag_{0.2}MXene_{0.8}$(b) and the corresponding EDS elemental mapping of (c) Ag and (d) Ti in the $Ag_{0.2}MXene_{0.8}$ nanocomposites. (e) TEM image of the $Ag_{0.2}MXene_{0.8}$ (The inserted magnified image shows the histogram for size distribution of Ag nanoparticles). (f) HRTEM image of the $Ag_{0.2}MXene_{0.8}$. (g) XRD patterns of pure MXene, $Ag_{0.2}MXene_{0.8}$, $Ag_{0.4}MXene_{0.6}$ and pure Ag. (h) Survey scan XPS spectra of pure MXene and $Ag_{0.2}MXene_{0.8}$. (i) Core-level XPS spectra of Ti element in pure MXene and $Ag_{0.2}MXene_{0.8}$. (j) Core-level XPS spectrum of Ag element in $Ag_{0.2}MXene_{0.8}$. (k) SEM image of the freeze-dried AM/Ch gel. (l) Different shapes kneaded from AM/Ch gel and Ch gel. (m) XRD patterns of chitosan power, freeze-dried Ch gel and AM/Ch gel.

2.2. Photothermal sterilization properties ofAg/MXene composites

The dispersion of Ag/MXene nanocomposites with different component ratios in water was shown in**Figure 2** a. The optical property investigation showed that Ag/MXene composites could efficiently absorb the light across the UV-Vis-IR region, hinting its high capacity for solar light utilization (Figure 2b). Therefore, their photo-to-thermal conversion efficiency was evaluated. Ag/MXene composites aqueous suspensions (150 μg mL^{-1}) were exposed to irradiation of 0.3 W cm^{-2}, and the real-time temperature was recorded

using an infrared thermal camera. In Figure 2c and Figure 2d, as the irradiation time grew, the temperature of Ag/MXene composites aqueous suspensions gradually increased. After 15 min of illumination, the temperature of MXene suspension went up to 55.2 °C ([?]T = 31.1 degC), while the temperature of $Ag_{0.2}/MXene_{0.8}$ reached 53.2 degC ([?]T = 29.2 degC), demonstrating that the introduction of Ag brought in no enhancement in photo-to-thermal conversion due to the inferior photothermal effect of silver nanoparticles. With the increase of silver content to 40%, the photothermal performance of the corresponding suspension decreased drastically, which could be attributed to the destruction of the lamellar structure of $Ag_{0.4}/MXene_{0.6}$(Figure S3a, Supporting Information). In contrast, the phosphate-buffered saline (PBS) exhibited negligible temperature change, which further confirmed that the temperature rise could be attributed to the photo-to-thermal conversion over MXene-based composites. Furthermore, the photo-induced heating curves of $Ag_{0.2}/MXene_{0.8}$for five cycles under the light on/off cycles demonstrated excellent photothermal stability (Figure 2e), showing its prospective potential for long-term photothermal applications.

Inspired by the outstanding photothermal properties of Ag/MXene composites, we evaluated their broad-spectrum antibacterial capability against Gram-positive *S. aureus* and Gram-negative *E. coli* in dark or under light through plate counting method (Figure S6, Supporting Information). As shown in Figure 4f-g, pure MXene and pure Ag both showed inferior killing effects against *E. coli* and *S. aureus* in dark. The low antibacterial behaviors of pure Ag nanoparticles may be attributed to the poor dispersion and heavy agglomeration in aqueous suspensions (Figure S3b, Supporting Information).[32] However, for the Ag/MXene composites, it could be clearly observed that the introduction of Ag could significantly decrease the survival rate of both *E. coli* and *S. aureus* , which was beneficial for the self-cleaning ability of the materials in dark. Given that the Ag/MXene composites will be used for photothermal purposes, we further evaluated the bacterial inhibition capacity of these composites under irradiation (0.3 W cm^{-2}), and the results indicated that both *E. coli* and *S. aureus* growth was dramatically inhibited and the survival rate was dramatically reduced correspondingly. For the MXene-based materials, over 90% of the bacteria were inactivated under the irradiation density of 0.3 W cm^{-2}, indicating the brilliant antibacterial effect of photothermal therapy (PTT) arising from the photothermal effect of MXene. Although Ag has been widely used as an antibacterial agent, its antibacterial effect is relatively low compared with MXene. However, when Ag and MXene are combined, especially $Ag_{0.2}/MXene_{0.8}$, showed much enhanced antibacterial efficiency compared to pure MXene, indicating the synergy between PTT and Ag^+ ions release in bacterial killing. Up to 99.76% of *E. coli* and 99.41% of*S. aureus* were killed within 15 min under irradiation of 0.3 W cm^{-2}. Additionally, it was evident that*E. coli* , as previously reported, was more susceptible to antibacterial treatments, which was owing to its thinner peptidoglycan layers of the cell wall in Gram-negative bacteria.[33,34]As discussed earlier, the synergistic bactericidal effect could be attributable to increased permeability of the bacterial cell membrane and sensitivity to heat by PTT, as well as the constant Ag^+ ions release from Ag nanoparticles which in-situ grew on $Ti_3C_2T_x$ lamellar structures. To further investigate the antibacterial mechanism, we used SEM to observe how *E. coli*and *S. aureus* morphology changed in response to various treatments. As shown in Figure 2h, both *E. coli* and *S. aureus,* before being treated (control group), showed smooth and intact cell membranes. However, after antibacterial treatment, the cell membrane of both *E. coli*and *S. aureus* showed severe wrinkles and damage with the presence of $Ag_{0.2}/MXene_{0.8}$, confirming the remarkable bactericidal activity. Based on the high photothermal effect, well-maintained 2D structure and superb bactericidal performance, $Ag_{0.2}/MXene_{0.8}$ (referred as Ag/MXene) was utilized to fabricate photothermal AM/Ch gel for solar steam generation.

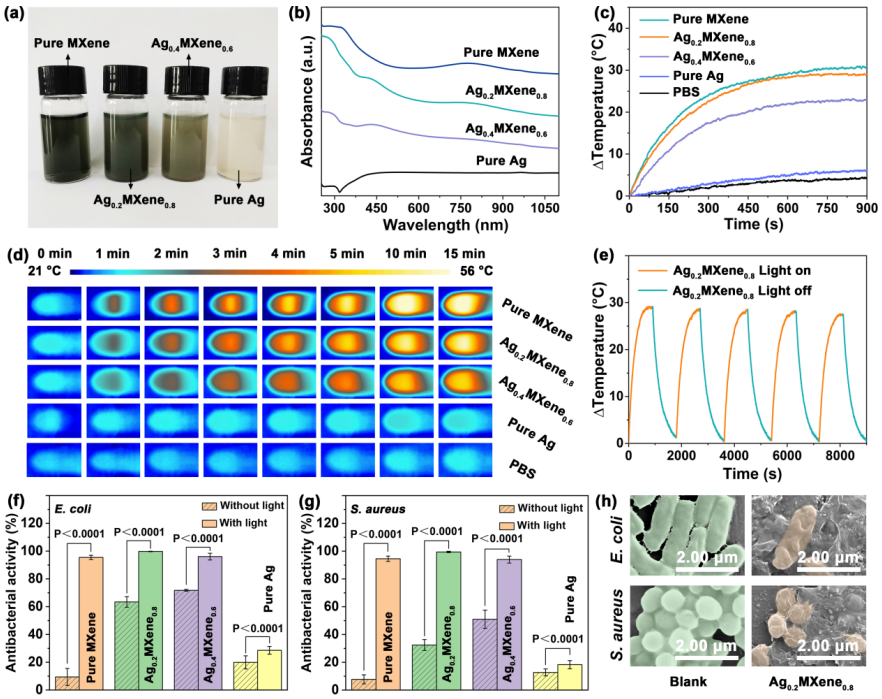

Figure 2. (a) Digital photo of aqueous suspensions of pure MXene, $Ag_{0.2}MXene_{0.8}$, $Ag_{0.4}MXene_{0.6}$ and pure Ag. (b) UV-Vis absorption spectra of pure MXene, $Ag_{0.2}MXene_{0.8}$, $Ag_{0.4}MXene_{0.6}$ and pure Ag. (c) Temperature changes of pure MXene, $Ag_{0.2}MXene_{0.8}$, $Ag_{0.4}MXene_{0.6}$, pure Ag and PBS buffer solution under irradiation (0.3 W cm^{-2}). (d) IR thermal images of pure MXene, $Ag_{0.2}MXene_{0.8}$, $Ag_{0.4}MXene_{0.6}$, pure Ag and PBS buffer solution. (e) Photothermal heating curves of $Ag_{0.2}MXene_{0.8}$ for five light on/off cycles (0.3 W cm^{-2}). Antibacterial activity against*E. coli* (f) and *S. aureus* (g) with pure MXene, $Ag_{0.2}MXene_{0.8}$, $Ag_{0.4}MXene_{0.6}$, and pure Ag in dark or under irradiation (0.3 W cm^{-2}). (h) SEM images of the dead *E. coli* and *S. aureus* treated with $Ag_{0.2}MXene_{0.8}$.

2.3. The photothermal sterilization andself-cleaning property of AM/Ch gel

Since in most cases, there are lots of microbes in seawater or polluted water, the sterilization capacity of AM/Ch gel solar evaporator is quite essential to ensure the production of clean and drinkable water. As such, we first evaluated the antibacterial effect of AM/Ch gel under irradiation of 0.2 W cm^{-2}, as illustrated in **Figure 3** a. As presented in Figure 3b–e, after being treated for 15 min, the pure chitosan hydrogel displayed a 9.23% antibacterial efficiency towards*E. coli* and a 8.14% antibacterial activity against *S. aureus* , respectively, which could be explained by inherent antibacterial properties of chitosan, brought by the numerous functional groups including positively charged quaternary ammonium salt groups that might interact with the negatively charged bacteria cell membranes to trap and inactivate pathogens.[35]In contrast, AM/Ch gel exhibited much enhanced bactericidal ability, with a killing rate of 58.34% against *E. coli* and 35.09% against *S. aureus* after 15 min treatment. After light irradiation for an extra 15 min, the pure chitosan hydrogel showed inferior antibacterial ability, killing only 74.31% of *E. coli*and 35.44% of *S. aureus* . Notably, all the *E. coli* and*S. aureus* were apparently inactivated after treatment with AM/Ch gel, which demonstrated its potential for producing bacteria-free clean water. The excellent antibacterial activity of AM/Ch gel was partially ascribed to the effect of PTT arising from MXene. Besides, the constant release of Ag^+ ions may contribute to the long-term antimicrobial effectiveness of AM/Ch gel system. Specifically, as shown in Figure 3f, the concentration of Ag^+ ions increased from 0 to 0.35 ppm in 15 min and achieved 0.70 ppm in 30 min under irradiation. As the Ag^+ ions concentration increased, the antibacterial activity against *E. coli* and *S.*

aureus both rose to 100% after 30 min irradiation. These results revealed that, with the synergistic effect of the chitosan hydrogel matrix (inherent sterilization) and Ag/MXene nanosheets (photothermal sterilization and Ag^+ ions release), the designed AM/Ch gel system exhibited robust antibacterial activity.

Except for the capacity to produce bacteria-free clean water, the self-cleaning antibacterial property of AM/Ch gel is also important for its recyclable and sustainable use, as shown in Figure 3g. To investigate its self-cleaning property, AM/Ch gel was first placed into a PBS buffer solution containing mixed bacteria of *E. coli* and *S. aureus* for 24 h (Figure 3h). The supernatant was then diluted for 10,000 times and coated on the Luria-Bertani (LB) medium for 18 h to quantify the number of colonies. The growth of colonies on LB media under various conditions was shown in Figure j-o. The treatment with AM/Ch gel significantly reduced the number of colonies, demonstrating its outstanding self-cleaning capacity. Figure 3i showed that the concentration of Ag^+ ions released from the hydrogel reached 15.01 ppm within 24 h, which might account largely for the high antibacterial behavior in the dark. In addition, the self-cleaning property of AM/Ch gel might also be attributed to the chitosan chains with intrinsic bacterial killing capacity originating from the abundant positive amino groups (NH_2), which could engage in electrostatic interaction with the negatively charged germs, killing them in the end.

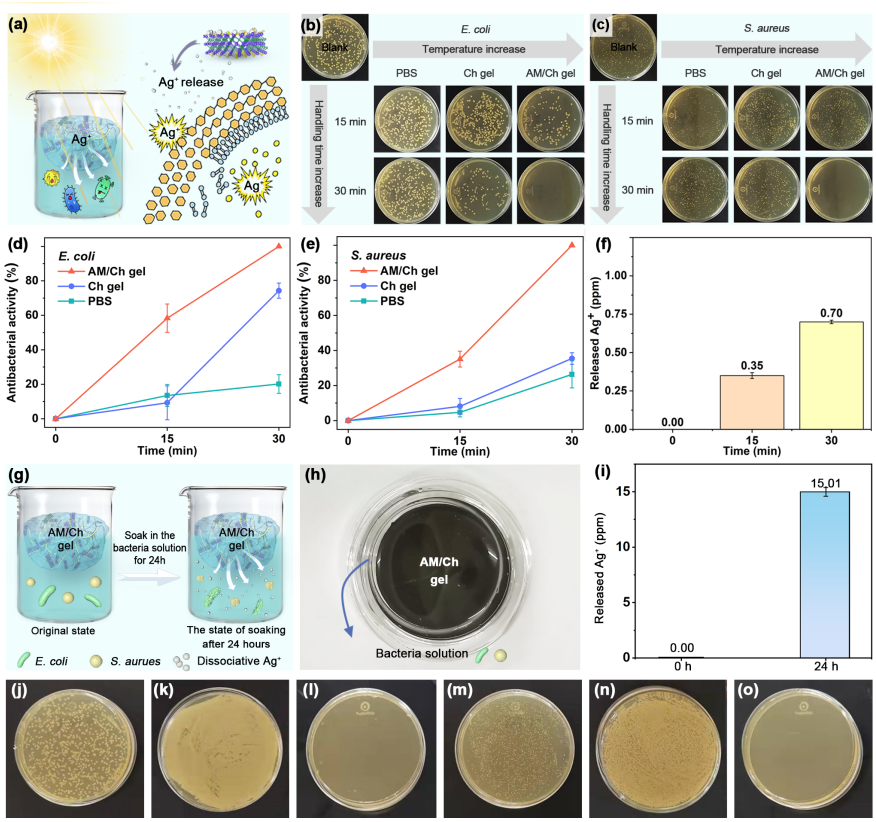

Figure 3. (a) Schematic diagram of the photothermal antibacterial mechanism of AM/Ch gel. Image of bacterial colonies formed by *E. coli* (b) and *S. aureus*(c) treated with PBS buffer solution, Ch gel and AM/Ch gel under irradiation (0.2 W cm^{-2}, 30 min). Curve of antibacterial activity of *E. coli* (d) and *S. aureus* (e) after treatment with PBS buffer solution, chitosan hydrogel and AM/Ch gel with time increasing. (f) Comparison of the concentration of Ag^+ ions released with time under irradiation (0.2 W cm^{-2}, 30 min). (g) Schematic diagram for self-cleaning process of AM/Ch gel. (h) Digital photo of AM/Ch gel soaked in a bacterial solution. (i) Comparison of the concentration of Ag^+ ions released in dark. Antibacterial tests: (j) spread plate results of *E. coli* from the original bacterial solution, (k) the untreated bacterial solution for 24

hour, and (l) the bacterial solution after treatment with AM/Ch gel for 24 hour; spread plate results of (m) *S. aureus* from the original bacterial solution, (n) the untreated bacterial solution for 24 hour, and (o) the bacterial solution after treatment with AM/Ch gel for 24 hour.

2.4. The water evaporation property of AM/Ch gel solar evaporator

Considering the superior photothermal performance of the Ag/MXene composites, the solar evaporation performance of the AM/Ch gel evaporator was investigated. As illustrated in **Figure 4** a, the water evaporation system was fabricated by the growth of the hydrogel on the top of expandable polyethylene (EPE) foam as a thermal insulator. An electronic analytical balance was utilized to quantify the change in water mass caused by the vapor escape. The filled AM/Ch gel in the two holes of EPE foam could act as sustained water transportation channels, mimicking the roots of trees in nature. During the water evaporation test, an IR camera was used to record the surface temperature of solar steam generator under light irradiation (incident angle: 0°). As shown in Figure 4b, the weight of water almost kept constant in dark, indicating that the natural evaporation could be negligible. And under light irradiation, the water evaporation was enhanced and the presence of chitosan hydrogel brought no further enhancement of steam generation. In comparison, the water weight in the presence of AM/Ch gel exhibited an almost leaner decrease as the irradiation time prolonged, an indicator of constant and stable steam generation. Figure 4c showed that the evaporation rate of the AM/Ch gel evaporator reached 3.22 kg $m^{-2}h^{-1}$, which was approximately 3.7 times for the Ch gel evaporator (0.86 kg m^{-2} h^{-1}) and 3.88 times compared to pure water control sample (0.83 kg $m^{-2}h^{-1}$). Similarly, the evaporation rate of the AM/Ch gel evaporator in seawater obtained from the Yellow Sea, China, was 3.10 kg $m^{-2}h^{-1}$, which was also much higher than the rate of natural evaporation (Figure S7a-b, Supporting Information). As shown in Figure 4d-e, the surface temperature of the device increased quickly and then stabilized for the irradiation period from 0 to 60 min. In particular, the surface temperature increased to 52.3 degC (T = 30.0 degC) over AM/Ch gel, which was considerably higher than Ch gel and pure water due to the strong photothermal effect of Ag/MXene composites. To assess the energy utilization potential of AM/Ch gel evaporator, the solar evaporation efficiency (η) was also calculated (Supporting Information). According to Figure S8a-b (Supporting Information), the evaporation efficiency of the AM/Ch gel evaporator could reach 94.9%, which was much higher than that of the Ch gel evaporator (22.8%) and even most photothermal evaporators previously reported in the past five years (Figure 4f and Table S1, Supporting Information). Such an excellent evaporation rate and energy conversion efficiency demonstrated the potential of AM/Ch gel for durable and sustainable water distillation, which could be mostly attributed to its outstanding photothermal conversion capability, lowered evaporation enthalpy, and sustained water molecules transportation in the networks.

The vapor generated by light irradiation was condensed, and the liquid water was collected to assess the purification effectiveness of AM/Ch gel evaporator. After being measured by inductively coupled plasma-optical emission spectrometry (ICP-OES), the concentrations of four primary ions (Na^+, Mg^{2+}, K^+ and Ca^{2+}) were greatly reduced by three to four orders of magnitude after desalination when we used the seawater samples from the Yellow Sea, China, (Figure 4g), which meet the requirement for drinking water quality on World Health Organization,[36] revealing the excellent performance of AM/Ch gel evaporator for seawater desalination. Furthermore, water evaporation experiments were also conducted using wastewater containing dyes as simulated contaminants, including methyl orange and methylene blue dyes. Figure 4h showed the color of the sewage turned transparent, and the strong absorption peaks of methyl orange (˜ 465 nm) and methylene blue (˜ 665 nm) were almost eradicated after purification with AM/Ch gel evaporator, showing its potential for clean water production from sewage.

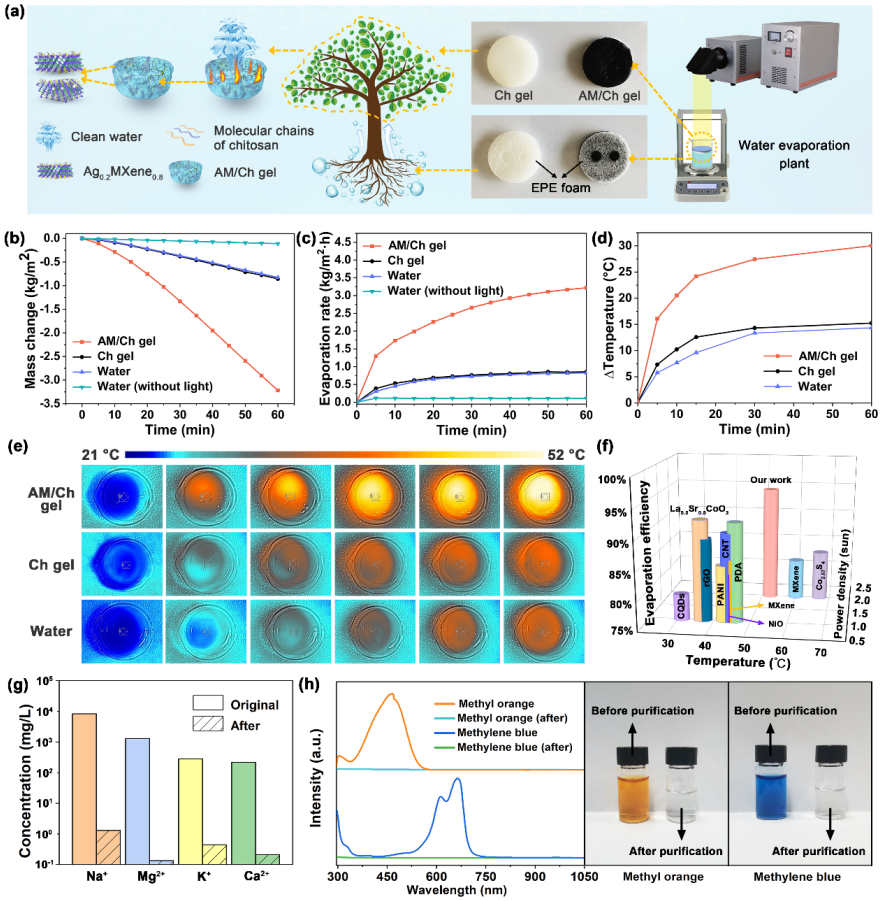

Figure 4. Solar vapor generation under irradiation of 0.2 W cm^{-2}. (a) A schematic diagram of the system for measuring water evaporation. (b) The mass change of water for AM/Ch gel, Ch gel and pure water. (c) The evaporation rate of the AM/Ch gel, Ch gel and pure water. (d) Temperature changes of the AM/Ch gel, Ch gel and pure water. (e) IR thermal images of the surface temperature of the AM/Ch gel, Ch gel and water with irradiation time. (f) A multi-dimensional comparison of AM/Ch gel evaporator with other photothermal material evaporators, including carbon quantum dots (CQDs),[37] $La_{0.5}Sr_{0.5}CoO_3$(LSC),[38] reduced graphene oxide (rGO),[39] polyaniline (PANI),[40] carbon nanotubes (CNT),[41] nickel oxide (NiO),[42] MXene,[43] $Co_{2.67}S_4$,[44] polydopamine (PDA).[45] (g) Concentration changes of Na^+, Mg^{2+}, K^+, and Ca^{2+} ions before and after treatment with AM/Ch gel evaporator. (h) Absorption intensity curve and digital photos of methyl orange and methylene blue contaminated water before and after evaporation purification.

3. Conclusion

In conclusion, by crosslinking chitosan chains through hydrogen bonding with Ag/MXene composites as additives, the obtained AM/Ch gel based solar steam generator exhibits features of high antibacterial and self-cleaning ability, satisfying solar energy conversion efficiency and promising clean water production capacity, due to the superb photo-to-thermal conversion behavior of Ag/MXene photothermal centers and feasible water transportation in the biomimetic 3D networks. As such, high solar steam generation rate of 3.22 kg $m^{-2}h^{-1}$ with a solar energy utilization efficiency of 94.9% has been achieved under irradiation of 0.2 W cm^{-2}, outperforming most of the previously reported solar evaporators. Besides, the concentrations of four primary ions (Na^+, Mg^{2+}, K^+ and Ca^{2+}) were reduced by three to four orders of magnitude after desalination using seawater samples from the Yellow Sea, China, meeting the requirement for drinking water quality according to World Health Organization, and this reveals the bright prospects of our AM/Ch gel

evaporator for seawater desalination.

Supporting Information

Supporting Information is available from the Wiley Online Library or from the author.

Acknowledgments

Shuyan Hao and Xintong Chen contributed equally to this work. This work was supported by the National Natural Science Foundation of China (Nos. 21902085, 52172213 and 82002793), the Natural Science Foundation of Shandong Province (ZR2020QH183) and Natural Science and Development Foundation of Shenzhen (JCYJ20190807093205660).

Conflict of Interest

The authors declare that they have no known competing financial interests or personal relationships that could have appeared to influence the work reported in this paper.

References

[1] M. Gao, L. Zhu, C. K. Peh, G. W. Ho, *Energy Environ. Sci.***2019** , *12* , 841.

[2] X. Guan, P. Kumar, Z. Li, T. K. A. Tran, S. Chahal, Z. Lei, C. Huang, C. Lin, J. Huang, L. Hu, Y. Chang, L. Wang, J. S. J. Britto, L. Panneerselvan, D. Chu, T. Wu, A. Karakoti, J. Yi, A. Vinu, *Adv. Sci.* **2023** , 2205809.

[3] T. Tao, K. L. Xin, *Nature* **2014** , *511* , 527.

[4] J. G. Liu, W. Yang, *Science* **2012** , *337* , 649.

[5] J. Qiu, *Science* **2011** , *334* , 745.

[6] X. Wu, J. Nan, J. Shen, J. Kang, D. Li, P. Yan, W. Wang, B. Wang, S. Zhao, Z. Chen, *J. Hazard. Mater.* **2022** , *428* , 128264.

[7] R. Y. K. Chang, S. C. Nang, H. Chan, J. Li, *Adv. Drug Deliv. Rev.***2022** , *187* , 114378.

[8] M. A. Shannon, P. W. Bohn, M. Elimelech, J. G. Georgiadis, B. J. Marinas, A. M. Mayes, *Nature* **2008** , *452* , 301.

[9] A. Subash, M. Naebe, X. Wang, B. Kandasubramanian, *J. Hazard. Mater.***2023** , *443* , 130168.

[10] Z. W. Lei, X. T. Sun, S. F. Zhu, K. Dong, X. Q. Liu, L. L. Wang, X. S. Zhang, L. J. Qu, X. J. Zhang, *Nano-Micro Lett.* **2022** , *14* , 10.

[11] P. Tao, G. Ni, C. Song, W. Shang, J. Wu, J. Zhu, G. Chen, T. Deng,*Nat. Energy* **2018** , *3* , 1031.

[12] S. Meng, C. Tang, J. Yang, M. Yang, W. Yang, *Adv. Sci.***2022** , *9* , 2204187.

[13] S. Santoro, A. H. Avci, A. Politano, E. Curcio, *Chem. Soc. Rev.***2022** , *51* , 6087.

[14] L. B. Zhang, B. Tang, J. B. Wu, R. Y. Li, P. Wang, *Adv. Mater.***2015** , *27* , 4889.

[15] J. Wang, Y. Li, L. Deng, N. Wei, Y. Weng, S. Dong, D. Qi, J. Qiu, X. Chen, T. Wu, *Adv. Mater.* **2017** , *29* .

[16] M. Yang, C. F. Tan, W. Lu, K. Zeng, G. W. Ho, *Adv. Funct. Mater.***2020** , *30* .

[17] P. P. Zhang, Q. H. Liao, T. Zhang, H. H. Cheng, Y. X. Huang, C. Yang, C. Li, L. Jiang, L. T. Qu, *Nano Energy* **2018** , *46* , 415.

[18] P. H. Yang, K. Liu, Q. Chen, J. Li, J. J. Duan, G. B. Xue, Z. S. Xu, W. K. Xie, J. Zhou, *Energy Environ. Sci.* **2017** , *10* , 1923.

[19] X. Wu, M. E. Robson, J. L. Phelps, J. S. Tan, B. Shao, G. Owens, H. L. Xu,*Nano Energy* **2019** , *56* , 708.

[20] Y. F. Gu, X. J. Mu, P. F. Wang, X. Y. Wang, J. Liu, J. Q. Shi, A. Y. Wei, Y. Z. Tian, G. S. Zhu, H. R. Xu, J. H. Zhou, L. Miao, *Nano Energy***2020** , *74* , 104857.

[21] Y. Lu, D. Fan, Y. Wang, H. Xu, C. Lu, X. Yang, *ACS Nano* **2021** ,*15* , 10366.

[22] Y. Shi, O. Ilic, H. A. Atwater, J. R. Greer, *Nat. Commun.***2021** , *12* , 2797.

[23] J. Zhou, S. Lin, H. Zeng, J. Liu, B. Li, Y. Xu, X. Zhao, G. Chen,*Mater. Horizons* **2020** , *7* , 2936.

[24] S. Hao, H. Han, Z. Yang, M. Chen, Y. Jiang, G. Lu, L. Dong, H. Wen, H. Li, J. Liu, L. Wu, Z. Wang, F. Wang, *Nano-Micro Lett.* **2022** ,*14* , 178.

[25] W. Wang, H. Feng, J. Liu, M. Zhang, S. Liu, C. Feng, S. Chen, *Chem. Eng. J.* **2020** , *386* , 124116.

[26] Y. W. Zheng, Y. L. Yan, L. M. Lin, Q. He, H. H. Hu, R. Luo, D. Y. Xian, J. Y. Wu, Y. Shi, F. P. Zeng, C. B. Wu, G. L. Quan, C. Lu, *Acta Biomater.* **2022** , *142* , 113.

[27] P. Xue, H. K. Bisoyi, Y. Chen, H. Zeng, J. Yang, X. Yang, P. Lv, X. Zhang, A. Priimagi, L. Wang, X. Xu, Q. Li, *Angew. Chem.-Int. Edit.***2021** , *60* , 3390.

[28] S. Chakraborty, H. Kumar, C. Dasgupta, P. K. Maiti, *Accounts Chem. Res.* **2017** , *50* , 2139.

[29] H. Pazniak, A. S. Varezhnikov, D. A. Kolosov, I. A. Plugin, A. Di Vito, O. E. Glukhova, P. M. Sheverdyaeva, M. Spasova, I. Kaikov, E. A. Kolesnikov, P. Moras, A. M. Bainyashev, M. A. Solomatin, I. Kiselev, U. Wiedwald, V. V. Sysoev, *Adv. Mater.* **2021** , *33* , 2104878.

[30] R. P. Pandey, K. Rasool, V. E. Madhavan, B. Aissa, Y. Gogotsi, K. A. Mahmoud,*J. Mater. Chem. A* **2018** , *6* , 3522.

[31] X. Huo, B. Zhang, J. Li, X. Wang, T. Qin, Y. Zhang, F. Kang, *ACS Appl. Mater. Interfaces* **2021** , *13* , 11822.

[32] X. Lv, L. Wang, A. Mei, Y. Xu, X. Ruan, W. Wang, J. Shao, D. Yang, X. Dong,*Small* **2022** , *19* , 2206220.

[33] H. Han, X. Xu, H. Kan, Y. Tang, C. Liu, H. Wen, L. Wu, Y. Jiang, Z. Wang, J. Liu, F. Wang, *J. Colloid Interface Sci.* **2022** ,*616* , 304.

[34] G. Fang, W. Li, X. Shen, J. M. Perez-Aguilar, Y. Chong, X. Gao, Z. Chai, C. Chen, C. Ge, R. Zhou, *Nat. Commun.* **2018** , *9* , 129.

[35] X. Ding, S. Duan, X. Ding, R. Liu, F. Xu, *Adv. Funct. Mater.***2018** , *28* , 1802140.

[36] World Health Organization, Guidelines for Drinking-water Quality,*https://www.who.int/publications/i/item/9789241548151,* accessed: Feb, **2023** .

[37] W. Chao, Y. Li, X. Sun, G. Cao, C. Wang, S. Ho, *Chem. Eng. J.***2021** , *405* , 126703.

[38] D. Fan, Y. Lu, H. Zhang, H. Xu, C. Lu, Y. Tang, X. Yang, *Applied Catalysis B: Environmental* **2021** , *295* , 120285.

[39] Z. Xiong, Y. Zhu, D. Qin, R. Yang, *ACS Appl. Mater. Interfaces***2020** , *12* , 32556.

[40] R. Li, C. Zhou, L. Yang, J. Li, G. Zhang, J. Tian, W. Wu, *J. Hazard. Mater.* **2022** , *424* , 127367.

[41] M. Jin, Z. Wu, F. Guan, D. Zhang, B. Wang, N. Sheng, X. Qu, L. Deng, S. Chen, Y. Chen, H. Wang, *ACS Appl. Mater. Interfaces***2022** , *14* , 12284.

[42] D. Qin, Y. Zhu, R. Yang, Z. Xiong, *Nanoscale* **2020** ,*12* , 6717.

[43] W. Qu, H. Zhao, Q. Zhang, D. Xia, Z. Tang, Q. Chen, C. He, D. Shu, *ACS Sustain. Chem. Eng.* **2021** , *9* , 11372.

[44] L. Zhao, Q. Yang, W. Guo, H. Liu, T. Ma, F. Qu, *ACS Appl. Mater. Interfaces* **2019** , *11* , 20820.

[45] Y. Sun, X. Zong, D. Qu, G. Chen, L. An, X. Wang, Z. Sun, *J. Mater. Chem. A* **2021** , *9* , 7122.

We report the fabrication of Ag/MXene@chitosan hydrogel as an antibacterial solar evaporator for clean water production. The porous networking structure enables light-trapping, photo-to-thermal conversion and water transportation, thus realizing high evaporation rate and solar energy utilization efficiency of 3.22 kg $m^{-2}h^{-1}$ and 94.9% under irradiation of 0.2 W cm^{-2}, respectively.

Shuyan Hao[1,#], Xintong Chen[1,#], Tingting Zhao[1], Yanyan Jiang[1], Hecheng Han[1], Jiurong Liu[1], Lun Dong[2,4*], Fenglong Wang[1,3,*]

Fabrication of antibacterial and biomimetic chitosan-based hydrogel embedded with Ag/MXene nanocomposites as photothermal centers for solar steam generation and desalination